This is a post-peer-review, pre-copyedit version of an article published in Nature Geoscience. The final authenticated version is available online at: http://dx.doi.org/10.1038/s41561-021-00783-4

Eruptive Activity of the Santorini Volcano Controlled by Sea Level Rise and Fall

Chris Satow[1]*, Agust Gudmundsson[2], Ralf Gertisser[3], Christopher Bronk Ramsey[4], Mohsen Bazargan[5], David M. Pyle[6], Sabine Wulf[7], Andrew J. Miles[8], Mark Hardiman[7].

[1]Department of Humanities and Social Sciences, Oxford Brookes University, Headington Road, Oxford, United Kingdom.
[2]Department of Earth Sciences, Royal Holloway University of London Egham, Surrey, United Kingdom
[3]School of Geography, Geology and the Environment, Keele University, Keele, United Kingdom
[4]School of Archaeology, University of Oxford, 1 South Parks Road, Oxford, United Kingdom
[5]Department of Earth Sciences, Uppsala University, Villavägen 16, Uppsala, Sweden
[6]Department of Earth Sciences, University of Oxford, South Parks Road, Oxford, UK
[7]School of the Environment, Geography and Geosciences, University of Portsmouth, Portsmouth, United Kingdom
[8] School of Geography, Geology and the Environment, University of Leicester, University Road, Leicester, UK
**correspondence: csatow@brookes.ac.uk*

Abstract

Sea-level change is thought to influence the frequencies of volcanic eruptions on glacial to interglacial timescales. However, the underlying physical processes and their importance relative to other influences (e.g. magma recharge rates), remain poorly understood. Here we compare a ~360 kyr long record of effusive and explosive eruptions from the flooded caldera volcano at Santorini (Greece) with a high resolution sea-level record spanning the last four glacial-interglacial cycles. Numerical modelling shows that when the sea level falls by 40 m below the present-day level, the induced tensile stresses in the roof of the magma chamber of Santorini trigger dyke injections. As the sea-level continues to fall to -70 or -80 m, the induced tensile stress spreads throughout the roof so that some dykes reach the surface to feed eruptions. Similarly, the volcanic activity gradually disappears after the sea-level rises above -40 m. Synchronising Santorini's stratigraphy with the sea-level record by using tephra layers in marine sediment cores shows that 208 out of 211 eruptions (both effusive and explosive) occurred during periods constrained by sea level falls (below -40m) and subsequent rises, suggesting a strong absolute sea-level control on the timing of eruptions on Santorini – a result that probably applies to many other volcanic islands around the world.

Climate as a Driver of Volcanism

The climate system's influence on solid-earth processes, including volcanic and tectonic activity[1-4] is receiving increasing attention from researchers. Changes in surface loading by growth and retreat of ice-sheets have been linked to changes in volcanic activity in formerly glaciated areas on timescales from 10^3 - 10^6 years[5-11]. Removal of an ice-sheet reduces the overburden pressure and results in additional decompression melting in the mantle. The associated stress changes in the crust facilitate dyke propagation to the surface, thereby increasing volcanic activity[10]. The effects of concomitant sea-level changes on volcanic activity, however, have not yet been firmly established. Because sea-level change is a worldwide phenomenon and the majority of the earth's volcanic systems are located in or next to oceans, this effect is of great global concern.

Previous studies of the effect of sea-level change on subaerial volcanic systems have been based only on ash layers preserved in marine sediment cores[12-14]. These studies have identified periods of greater eruptive activity that appear cyclical on Milankovitch timescales of 41 and 100 kyr [13,14]. Most volcanic systems, however, are not dominated by large explosive, ash-producing eruptions but by lava effusion and/or minor explosive activity, neither of which are represented in marine sediment core records. As a result, no studies have yet been able to compare the full range of eruptive activity from a single subaerial volcano to a sea-level record. The physical mechanisms that could link changes in sea-level and volcanic activity also remain elusive, with periods of increased explosive activity variously attributed to high rates of sea-level change[12], absolute sea-level changes through Milankovitch cycles[13-16], or increased melt production in the mantle[17].

To correlate sea-level changes with volcanic activity requires a well-dated volcanic system with a long and detailed proximal and distal record of both explosive and effusive eruptions, extending over more than one glacial-interglacial sea-level cycle. Santorini volcano, Greece (Supplementary Information Figure 1), satisfies all of these requirements. It has an unusually long, precisely dated and accessible record of major explosive (Plinian) eruptions and chronologically well-constrained intervals of lava effusion and minor explosive (interplinian) eruptions[18-20]. Santorini also benefits from the exceptional chronological control afforded by ash layers preserved in nearby marine sediment cores[21,22] (Supplementary Information Figure 1). Crucially for this study, these ash layers have been dated[22] with the same chronology as a recent, global sea-level curve[23,24], allowing direct alignment of the volcanic stratigraphy to the sea-level record and ensuring the most precise synchronisation of the two records possible.

The eruption time series for Santorini

Figure 1 shows the detailed eruption chronology of Santorini from ~360 ka to the present day. On the basis of long-term trends in magma composition, the eruption history has traditionally been split into two cycles[18,25]. Each cycle starts with effusive eruptions of low or intermediate silica content and ends with major silicic eruptions and a caldera collapse. The volcano is now, after the famous Late Bronze Age eruption[26,27], in its third cycle. These cycles are recorded in detail by the stratigraphy of the caldera walls (the islands of Thira and Thirasia, Supplementary Information Figure 1), where deposits originating from twelve major explosive (Plinian) eruptions, minor explosive (interplinian) eruptions and lava eruptions are evident.

A detailed chronology for the volcano[18,22,25] reveals long periods of quiescence which are marked by palaeosols and a notable absence of volcanic deposits (Fig. 1). While studies have explored magma-system controls on the nature of individual eruptions[26,28,29], the factors controlling the start and end of eruptive and quiescent phases have not been determined. Internal forcing such as increased magma flux into a magma chamber or external forcing such as the changes in crustal loading during glacial-interglacial cycles[13-16,30] may both play a role, but the relative importance of those roles has not yet been established.

Geophysical, petrological and geochemical results provide compelling evidence for the existence of a shallow magma chamber at the depth of about 4 km beneath Santorini's caldera[19,25,29,31-35]. To simulate the influence of sea-level loading, we present the results of numerical modelling (Fig. 2; Supplementary Information Figure 2) which indicate that stress changes due to changes in sea-level during the Late Quaternary are sufficient to trigger (during low sea-level) or inhibit (during high sea-level) dyke injection from the magma chamber. We test our model results by integrating Santorini's volcanic stratigraphy with a eustatic sea-level record[23,24] (and also rates of sea-level change- Supplementary Information Figure 3) spanning four glacial-interglacial cycles. The empirical evidence supports our model, suggesting that eustatic sea-level-induced stress changes over the past 360 kyr largely controlled dyke injections from the shallow chamber and, therefore, the timing of periods of eruptive activity.

Modelling the effect of sea-level changes on dyke injection and eruptions

When global sea-level rises, the load on the crust/lithosphere increases; when the sea-level falls, the load decreases. The load here is the vertical stress due to the hydrostatic pressure of the sea water. Hydrostatic pressure p is given by $p = \rho g z$ where ρ is the water density, g is the acceleration due to gravity, and z is the depth below the surface of the water. Using the average sea-water density of 1025 kgm^{-3} and the acceleration due to gravity of 9.8 ms^{-2}, it follows that for every 10 m that the sea-level rises/falls the hydrostatic pressure or vertical stress changes by about 0.1 MPa, which translates into changes in crustal stresses[36,37] . In the vicinity of a magma chamber, increases in horizontal compressive stresses tend to inhibit, while increases in horizontal tensile stresses encourage, dyke injections from the chamber[37]. Rock tensile strength is almost constant to a crustal depth of 9 km (mostly 1-6 MPa, with an average of about 3.5 MPa[36]), so we assume that it does not vary in our model. If (as at Santorini) the crust hosts a shallow magma chamber the tensile stresses induced by sea-level fall become magnified (Fig. 2).

To simulate the effect of sea-level changes on the potential for dyke injections and eruptions, we used the software Comsol Multiphysics (www.comsol.com) to model associated changes in tensile stress concentration around the shallow magma chamber of the Santorini volcano. To explore how the tensile stress concentration in the roof of the chamber (controlling dyke propagation) changes during the fall in sea-level, we decreased the vertical stress in steps of 0.1 MPa, corresponding to sea-level falls of 10 m. This is the only loading in the model runs. Using the contemporary mean sea-level as the starting point (0 m), the final sea-level in the model is the one associated with the last glacial maximum at ~22 ka, namely -110 m. The initial (0 m) and final (-110 m) levels cover the entire range of Quaternary sea-level changes. We model the shallow magma chamber at 4 km depth as a 6 km-wide (horizontal dimension) sill-like flat ellipsoid and initially (at 0 m sea-level, the starting point in the model) in lithostatic equilibrium with the host rock. These assumptions as to geometry and lithostatic equilibrium are in line with geophysical observations[34,35] and previous magma-chamber modelling studies[28,37]. In the model, the crust hosting the chamber is layered (Fig. 2). We use typical 'seismic' layers, each 500 m thick and with increasing stiffness (Young's modulus) with depth, as is normal in volcanic areas[37].

The modelling results (Fig. 2) show how the induced tensile stress gradually spreads from the margin of the chamber and throughout the entire roof up to the surface as the sea-level falls in steps of 10 m from its initial (0 m) to its lowest (-110m) level. Dyke injection from a chamber occurs when the following condition is satisfied: $p_l + p_e = \sigma_3 + T_0$, where p_l is the lithostatic pressure, p_e is the magmatic excess pressure in the chamber with reference to σ_3, the minimum compressive principal stress in the roof next to the chamber, and T_0 is the in-situ (field) tensile strength of the roof[37]. Initially the chamber is in lithostatic equilibrium with the host rock, so that p_e is zero and no dykes are injected. As the sea-level falls, tensile-stress concentration around the chamber reduces σ_3 thereby increasing p_e. When the excess pressure p_e reaches the tensile strength of the roof, T_0, the roof ruptures and a dyke is injected. The excess pressure p_e must reach the average tensile strength of 3.5 MPa for a dyke to be injected.

The numerical modelling (Fig. 2; Supplementary Information Figure 2) shows that the tensile stress in the roof next to the chamber, hence p_e, reaches the absolute value of 3.5 MPa when the sea-level has fallen to about -40 m (40 m below the current level). Thus, magma-chamber rupture and dyke injection is encouraged once the sea-level has fallen by 40 m. At this sea-level, however, the tensile stress is limited to the vicinity of the chamber. Consequently, at this stage the injected dykes become arrested close to the magma chamber and do not reach the surface to supply magma to eruptions[37]. As the sea-level continues to fall below -40 m the induced tensile stress gradually spreads throughout the entire roof of the magma chamber. There is therefore an expected time-lag between the first dykes injected during a sea-level fall and the first dyke-fed eruptions at the surface (Figs. 2 and 3). Quantifying and explaining this time-lag is important in order to establish a complete understanding of how volcanism at Santorini, and subsequently other volcanic islands, reacts to sea level changes.

A time-lag between first sea-level triggered dyke injections and first dyke-fed eruptions

Time-lags between external forcing and volcanic response have been inferred in many previous studies. For basaltic volcanism in eastern California, the lag between glacial unloading and peak volcanism is defined as 11.2± 2.3 kyr[7]. Also, the peak in explosive volcanism in the Izu Bonin Arc (western Pacific Ocean) apparently lags behind the glacial maximum (sea-level minimum) by approximately 7 kyr[15]. Similarly, in Iceland the peak in late glacial and early Holocene volcanism occurred several thousand years after the deglaciation began[5, 10]. Some of these time-lags have been attributed to viscoelastic behaviour of the crust. However, the response of a crustal segment hosting a magma chamber is normally elastic to a first approximation[37-40]. Our model (fig. 2) is thus elastic. Since volcanic eruptions usually occur with unrest (inflation/deflation) periods[37] ,rather than hundreds or thousands of years after the unrest took place, viscoelastic behaviour of the crust[17] cannot be used to explain the long time-lags between glacial or sea-level unloading of the crust in volcanic areas and subsequent peaks in the numbers of eruptions.

Our model (Figs. 2 and 3) indicates instead that such long time-lags are a direct consequence of the evolution of the stress field in the roof of the magma chamber during the gradual change in external loading (Figs. 2 and 3). When the sea-level falls to -40 m, induced tensile stress concentration encourages dyke injection and propagation into the lower part of the roof of the chamber (Figs. 2 and 3). However, the stress in the upper part of the roof, closer to the surface, is still unfavourable to dyke propagation, so that the dykes become arrested (cf. 37, 40). As the sea level continues to fall further, greater parts of the roof become subjected to tensile stress (Figs. 2 and 3) so that the probability of an injected dyke reaching the surface to erupt increases. Similarly, when the sea level rises again, the tensile stresses gradually become suppressed (not shown in Fig. 2) until sea-level triggered dyke injections stop. There is thus an expected time-lag between the initiation of sea-level induced local stress fields favourable/unfavourable to dyke injections and the initiation/suppression of dyke-fed eruptions.

For Santorini, this time-lag can be quantified by using the period of eruptive activity (Fig. 4) constrained between the Plinian Lower Pumice 2 eruption at 176.7 +/- 0.6 ka[20] and the interplinian M9-2 eruption at 121.8 +/- 2.9 ka[22]. This eruption period is used not only because of the very precise dates defining its start and end[22], but also because these eruption dates are defined using ash layers in marine sediment cores (Supplementary Information Figure 1) which share the same chronology as the sea-level record[22-24], thereby eliminating the chronological uncertainty which would be otherwise be introduced by aligning two separate chronologies.

Sea-level drops below -40 m (when dyke-injection begins; Figs. 2 and 3) at 189.5 +/- 2.4 ka (Fig. 4) and rises back through -40 m at 132.5 +/- 2.1 ka[24]. The time-lag between the sea-level falling below -40 m and the start of eruptive activity (modelled at 70-80 m, fig. 2) marked by the Lower Pumice 2 eruption at 176.7 +/- 0.6 ka[20] is therefore 12.8 +/- 2.5 kyr. This reflects the time it usually takes for the sea-level to fall from -40 m to –70 m or -80 m (Figs. 3 and 4).

If the mechanical conditions were exactly the same during the rise and fall of the sea level, our elastic model would predict dyke arrest and no eruptions after sea-level rise through -40m (fig. 3). But the rise in sea-level is much faster (Fig. 4), and thus at a higher strain rate, than the fall. Also, during the rise above -40 m (but not during the fall below -40 m) there exist recently formed feeder-dykes (Fig. 3), some of which are still hot and perhaps partly molten close to the chamber. We suggest that these different conditions explain why during sea level rise eruptions stop at sea level of 0 m (marked by the M9-2 eruption at 121.8 +/- 2.9 ka); 10.7 +/- 3.6 kyr) rather than at -40 m at 132.5 +/- 2.1 ka. This combination of high strain rate, hot/partly molten dyke rock, and associated tensile stress concentrations is suggested here to encourage dyke-fed eruptions even after the sea-level has risen above -40 m.

Both time-lags (10.7 +/- 3.6 kyr for eruptions ceasing after sea level rises through -40 m and 12.8 +/- 2.5 kyr for eruptions starting after sea level falls through -40 m) have been extrapolated (Fig.4) throughout the ~360 kyr chronology of Santorini used here. This defines periods (bracketed by sea level rise and fall) where eruptions may be attributed solely to the changes in tensile stress caused by sea level changes.

Periods of eruptive activity constrained by a sea-level threshold

Our numerical results of sea-level induced stress changes around Santorini's shallow magma chamber (Figs. 2 and 3) indicate that eruptive activity will start 12.8 +/- 2.5 kyr after the sea level has fallen below -40 m (when the sea-level is at -70 m or -80 m) and cease about 10.7 +/- 3.6 kyr after sea level has risen above -40 m. Figure 4 shows that all but 3 of the 211 deposits (of all eruptive styles; Plinian, interplinian and lava) counted within the Santorini stratigraphy (between 224 ka and the present day) were erupted during such periods. Only one minor (interplinian) and two major (Plinian) explosive eruptions occurred outside of these periods. This pattern also appears to extend to the older and less well preserved part of Santorini's volcanic record (older than 224 ka, Fig. 4) where it is not possible to quantify the exact number of eruptions, or the dating is less precise. Prior to 224 ka, all known eruptions occurred during such periods. The lack of evidence for eruptive activity outside of these periods indicates that absolute sea-level exerts a fundamental control on the timing of eruptions at the Santorini volcano, by modulating the tensile stress and therefore dyke propagation above the magma chamber.

Implications for volcanic hazards

Cycles in eruptive composition and behaviour have long been recognised at Santorini[18,25] with the second explosive cycle culminating in the famous Late Bronze Age, or Minoan, eruption. The volcano is now considered to be at the start of its third cycle (Figs 1 and 4) and minor, effusive interplinian eruptions are thought to be the most likely hazard[25,31,43]. Our new analysis adds considerably to the understanding of these cycles by revealing that the timing of periods of eruptions is primarily controlled by changes in sea-level. This in turn indicates that the volcano will shortly enter a period of long-term repose; sea-level last rose through -40 m at 11.2 +/- 0.7 ka[23,24] and the time-lag between this sea-level and cessation of minor (effusive) eruptions (lava and interplinian in Fig. 4) is estimated here to be 10.7 +/- 3.6 kyr. Santorini volcano is therefore currently within the uncertainty range of this study's predicted cessation of effusive eruptive activity. It has been dormant since the 1950 eruption of Nea Kameni[25,41,42] (Fig. 1) and magma injected into the Santorini magma chamber in 2011-2012[34,41-43] failed to cause an eruption, hinting that this period of quiescence may already have begun. However, the eruptive record (Fig. 4) shows that two major explosive 'Plinian' eruptions (Cape Therma 3 and Lower Pumice 1; Fig. 1) occurred outside periods subjected to sea levels of below -40 m (accounting for the time-lags) and therefore that such large eruptions may remain a present-day threat. Nonetheless, the timing of 208 out of 211 eruptions recorded in the highly detailed volcanic stratigraphy at Santorini can be explained by the mechanism of dyke injection and propagation resulting from the tensile stresses induced by low sea levels.

Around 57% of the world's sub-aerial volcanoes are islands or on coasts[12], and therefore potentially affected by sea-level induced stress changes. The precise effects of sea-level changes on any particular volcanic system will depend on the geometry and depth of the source magma chamber and the mechanical properties of the crustal segment hosting the chamber. Comparative studies of other systems are vital to provide a general framework for making individual volcanic hazard assessments[14]. Such assessments are often set within the context of past eruptive timing. This study, however, implies that the unusually stable sea level of the Holocene and likely sea-level rise in the future (due to anthropogenic climate change) may render simple extrapolation of past eruption, timings into the future inaccurate. Instead, the eruptive history of any volcanic systems where sea-level variations may induce local stress-field changes should be examined within the context of a sea-level record to better infer their likely future eruptive behaviour.

The chronology of the Santorini volcano has allowed us, for the first time, to establish a clear relationship between sea-level change and the timing of eruptions of an active, subaerial volcano. Our results should encourage all island volcanic systems around the world to be examined within the context of sea-level induced stress changes around active magma chambers.

Acknowledgements and funding

CBR received funding from NERC in support of the NERC Isotope Facility. DMP acknowledges support from the NERC Centre for the Observation and Modelling of Earthquakes, Volcanoes, and Tectonics (COMET). MB acknowledges financial support from the Swedish Research Council (2018-03414) and the Weld On Sweden Research and Development Section. The authors thank the two excellent reviewers who greatly improved the quality of the manuscript. CS dedicates his contribution to this paper to Amy and Rory.

Competing Interests Statement

The authors declare no competing financial interests.

Author Contributions

CS: designed the study, co-compiled the eruption counts and co-wrote the paper. Co-produced figures 2 and 4 (main text) and Supplementary Information figures 2 and 3.
AG: Led numerical modelling, co-wrote the paper and produced figure 3.
RG: Wrote methods sections on stratigraphy, produced figure 1 and co-complied the eruption counts.
CBR: Undertook age modelling and produced the kernel density estimates (Figure 4 main text and Supplementary Information figure 3).
DP: Co-wrote the paper and advised on hazards information.
MB: Undertook the numerical modelling, co-produced figure 2 (main text) and Supplementary Information figure 2.
SW: Advised on eruption dates and the tephrostratigraphy of Santorini, and produced Supplementary Information figure 1.
AM: Conducted an internal review of the paper, contributed to project design and edited the final submission
MH: Co-produced figure 4 and Supplementary Information figure 3, and commented on the manuscript

Data Availability

Supplementary information (three diagrams and two data tables) and an Oxcal (.txt) file from which the kernel density estimate plots (fig. 4 and Supplementary figure 3) were created are available in the online version of the paper. These datasets are also available on the PANGAEA repository at: [insert DOI during proofing]. Reprints and permissions information is available online at www.nature.com/reprints. Correspondence and requests for materials should be addressed to C.S.

References

1. Matthews, R.K. Tectonic implications of glacio-eustatic sea-level fluctuations. *Earth Planet. Sci. Lett.* **5**, 459–462 (1969).

2. Rampino, M. R., Self, S. & Fairbridge, R. W. Can rapid climate change cause volcanic eruptions? *Science* **206**, 826–828 (1979).

3. Paterne, M. and Guichard, F. Triggering of volcanic pulses in the Campanian area, South Italy, by periodic deep magma influx. *J. Geophys. Res.* **98**, 1861-1873 (1993).

4. Mason, B.G. et al. Seasonality of volcanic eruptions, *J. Geophys. Res.* **109**, B04206 (2004).

5. Gudmundsson, A. Mechanical aspects of postglacial volcanism and tectonics of the Reykjanes Peninsula, southwest Iceland. *J. Geophys. Res*. **91**, 12,711-12,721 (1986).

6. Jull, M. and McKenzie, D. The effect of deglaciation on mantle melting beneath Iceland. *J. Geophys. Res*. **101**, 21815-21828 (1996).

7. Jellinek, M.A., Manga, M., and Saar, M. Did melting glaciers cause volcanic eruptions in eastern California? Probing the mechanics of dike formation. *J. Geophys. Res*. doi:10.1029/2004JB002978 (2004).

8. Nowell, D.A.G., Jones, M.C. and Pyle, D.M. Episodic Quaternary Volcanism in France and Germany. *J. Quat. Sci*. **21**, 645-675 (2006).

9. Watt, S.F.L., Pyle, D.M. and Mather, T.A. The volcanic response to deglaciation: evidence from glaciated arcs and a reassessment of global eruption records. *Earth Sci. Rev.* **122**, 77-102 (2013).

10. Andrew, R.E.B., Gudmundsson, A. Distribution, structure, and formation of Holocene lava shields in Iceland. *J. Volcanol. Geotherm. Res*., **168**, 137-154 (2007).

11. Rawson, H. et al. The magmatic and eruptive response of arc volcanoes to deglaciation: insights from southern Chile. *Geology* **44**, 251-254, doi:10.1130/G37504.1 (2016).

12. McGuire et al. Correlation between rate of sea-level change and frequency of explosive volcanism in the Mediterranean. *Nature* **389** pp473-476 (1997).

13. Kutterolf, S. et al. A detection of Milankovitch frequencies in global volcanic activity. *Geology* doi:10.1130/G33419.1 (2012).

14. Kutterolf, S. et al. Milankovitch frequencies in tephra records at volcanic arcs: The relation of kyr-scale cyclic variations in volcanism to global climate changes. *Quart. Sci. Rev.* **204**, 1-16 (2019).

15. Schindlbeck et al. 100 kyr cyclicity in volcanic ash emplacement: evidence from a 1.1 Myr tephra record from the NW Pacific. *Scientific Reports* DOI:10.1038/s41598-018-22595-0 (2018).

16. Stewart, I.S. Did sea-level change cause the switch from fissure-type to central-type volcanism at Mount Etna, Sicily? *Episodes* **41**, 7-16 (2018).

17. Sternai, P., et al. Magmatic pulse driven by sea-level changes associated with the Messinian salinity crisis. *Nat. Geo.* DOI: 10.1038/NGEO3032 (2017).

18. Druitt.T.H et al. Explosive volcanism on Santorini, Greece. *Geol. Mag.* **126,** 95-126 (1989).

19. Druitt, T.H., Pyle, D.M. and Mather, T.A. Santorini Volcano and its Plumbing System. *Elements* **15**, 177-184, doi: 10.2138/gselements.15.3.177 (2019).

20. Satow et al. Detection and Characterisation of Eemian Marine Tephra Layers within the Sapropel S5 1 Sediments of the Aegean and Levantine Seas. *Quaternary* **3** doi:10.3390/quat3010006 (2020)

21. Satow et al. A new contribution to the Late Quaternary tephrostratigraphy of the Mediterranean; Aegean Sea core LC21. *Quart. Sci. Rev.* **117***,* 96-112 (2015).

22. Wulf, S. et al. Advancing Santorini's tephrostratigraphy: new glass geochemical data and improved marine-terrestrial tephra correlations for the past ~360 kyrs. *Earth Sci. Rev*. https://doi.org/10.1016/j.earscirev.2019.102964 (2020).

23. Grant et al. Rapid coupling between ice volume and polar temperature over the past 150,000 years. *Nature* **491**, 744-747 (2012).

24. Grant et al. Sea-Level variability over 5 glacial cycles. *Nat. Commun.* **5** 5076 DOI: 10.1038/ncomms6076 (2014).

25. Druitt, T.H., et al. Santorini volcano. *Geol. Soc. Lond*. Mem. **19**, 1-165 (1999).

26. Druitt et al. Decadal to monthly timescales of magma transfer and reservoir growth at a caldera volcano. *Nature* doi:10.1038/nature10706 (2012).

27. Nomikou, P et al. Post-eruptive flooding of Santorini caldera and implications for tsunami generation. *Nature Commun.* DOI: 10.1038/ncomms13332 (2016).

28. Browning**.** et al. Forecasting magma chamber rupture at the Santorini Volcano, Greece *Nature Sci. Rep.* **5, 15785 DOI: 10.1038/srep15785** (2015).

29. Fabbro, G.N., Druitt, T.H. and Costa, F. Storage and eruption of silicic magma across the transition from dominantly effusive to caldera-forming states at an arc volcano (Santorini, Greece). *J. Petrol.* **58**, 2429-2464 (2017).

30. Wallman, P., Mahood, G. A., and Pollard, D.D. Mechanical models for correlation of ring fracture eruptions at Pantelleria, Strait of Sicily, with glacial sea-level drawdown. *Bull. Volcanol.* **50**, 327-339 (1988).

31. Parks, M.M., Biggs, J., England, P., Mather, T.A., Nomikou, P., Palamartchouk, K., Papanikolaou, X., Paradissis, D., Parsons, B., Pyle, D.M., Raptakis, C., Zacharis, V. Evolution of Santorini volcano dominated by episodic and rapid fluxes of melt from depth. Nature Geoscience 5, 749-754 (2012)

32. Hooft et al. Seismic imaging of Santorini: Subsurface constraints on caldera collapse and present-day magma recharge*. Earth. Planet. Sci. Lett*. **514**, 48-61 (2019).

33. Druitt, T.H. et al. Magma storage and extraction associated with Plinian and interplinian activity and Santorini Caldera (Greece) *J. Petrol.* **57,** 461-494 (2016).

34. Parks, M.M., et al. From quiescence to unrest - 20 years of satellite geodetic measurements at Santorini volcano, Greece. *J. Geophys. Res.* (Solid Earth), **120**, 1309-1328, doi:10.1002/2014JB011540 (2015).

35. McVey et al. Magma accumulation beneath Santorini volcano, Greece, from P-wave tomography. Geology **48:** 231-235 (2020).

36. Gudmundsson, A. Rock fractures in geological processes. Cambridge University Press, Cambridge (2011).

37. Gudmundsson, A. *Volcanotectonics: Understanding the structure, deformation and dynamics of volcanoes* (Cambridge Univ. Press, Cambridge, 2020).

38. Dzurisin, D. *Volcano deformation: new geodetic monitoring techniques* (Springer Verlag, Berlin, 2006).

39. Segall, P. *Earthquake and volcano deformation*. Princeton Univ. Press, Princeton, 2010).

40. Gudmundsson, A. Emplacement and arrest of dykes and sheets in central volcanoes. *J. Volanol. Geotherm. Res.* **116**, 279-298 (2002).

41. Parks, M.M. et al. Evolution of Santorini volcano dominated by episodic and rapid fluxes of melt from depth. *Nature Geosci*. **5**, 749-754 (2012).

42. Parks, M.M. et al. Distinguishing contributions to diffuse CO_2 emissions in volcanic areas from magmatic degassing and thermal decarbonation using soil gas ^{222}Rn-$\delta^{13}C$ systematics: application to Santorini volcano, Greece. *Earth Planet. Sci. Lett*. **377-378**, 180-190 (2013).

43. Newman et al. Recent geodetic unrest at Santorini Caldera, Greece. *Geophys. Res. Lett.* **39** doi:10.1029/2012GL051286 (2012).

44. Edwards, L., Magma cyclicity and isotopic variation on Santorini volcano, Aegean Sea, Greece. Ph.D. Thesis University of Bristol, UK (1994).

45. Vespa. M et al. Interplinian explosive activity of Santorini volcano (Greece) during the past 150,000 years. *J Volcanol. Geotherm. Res.* **153,** 262-286 (2006).

46. Karátson, D. et al. Towards reconstruction of the lost Late Bronze Age intra-caldera island of Santorini, Greece. Nature Sci. Rep **8**. (2018) https://doi/10.1038/s41598-018-25301-2.

47. Fabbro, G., Druitt, T.H., Scaillet, S. Evolution of the crustal magma plumbing system during the build-up to the 22-ka caldera forming eruption of Santorini (Greece), *Bull Volcanol*. **75**:767 DOI 10.1007/s00445-013-0767-5 (2013).

48. Vakhrameeva, P. et al. The cryptotephra record of the Marine Isotope Stage 12 to 10 interval (460-335 ka) at Tenaghi Philippon, Greece: Exploring chronological markers for the Middle Pleistocene of the Mediterranean region. Quat. Sci. Rev. 200, 313–333. (2018)

Main Text Diagrams

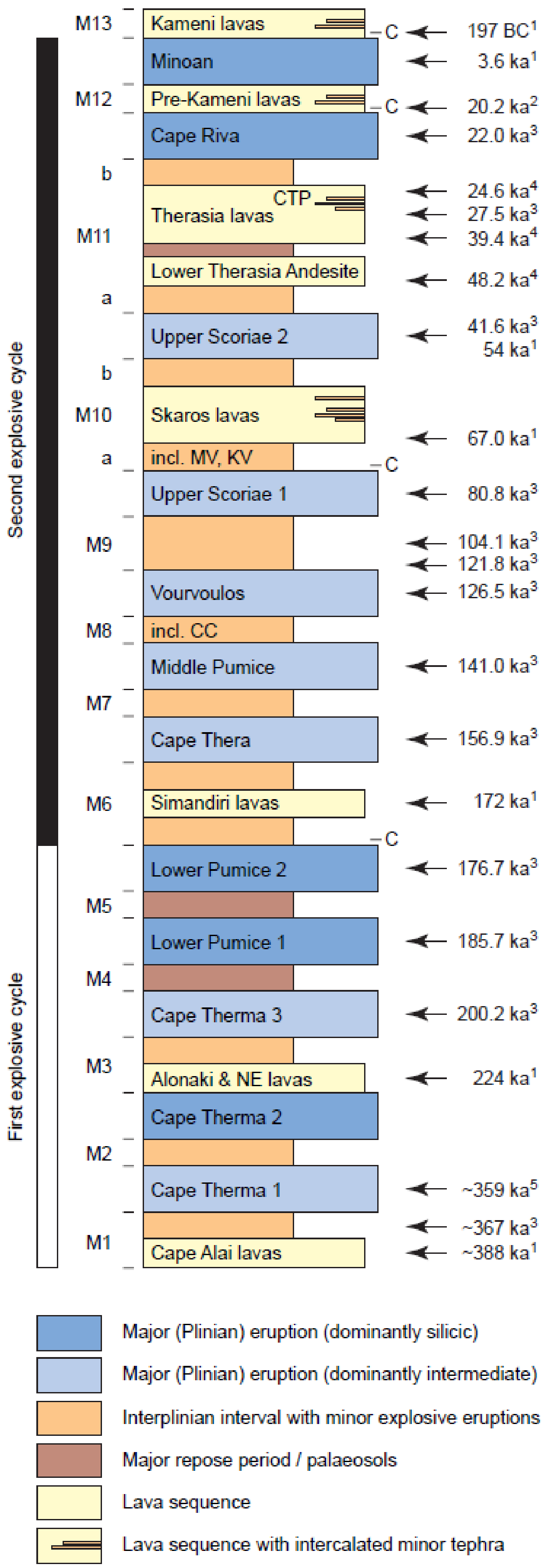

Figure 1. Stratigraphy and eruption chronology of Santorini from ~360 ka to the present, showing the twelve major explosive (Plinian) eruptions of Santorini (blue boxes) and divided into two explosive cycles. Episodes of caldera formation are marked by “C”. Interplinian intervals (M1 to M13) are characterized by minor explosive eruptions, cinder cones/tuff rings (MV = Megalo Vuono cinder cone; KV = Kokkino Vuono cinder cone; CC = Cape Columbos tuff ring), lava sequences (lava flows, shields and domes), and major repose periods marked by palaeosols or weathering horizons. Deposits from minor explosive eruptions, including the widespread Cape Tripiti Pumice (CTP) within the Therasia dome complex, and palaeosols which mark major periods of repose also occur within the major lava sequences. Citations for dates are as follows: 1[25], 2[46], 3[22], 4[46], 5[48]. 2σ uncertainties on these dates vary, but are often below 5%.

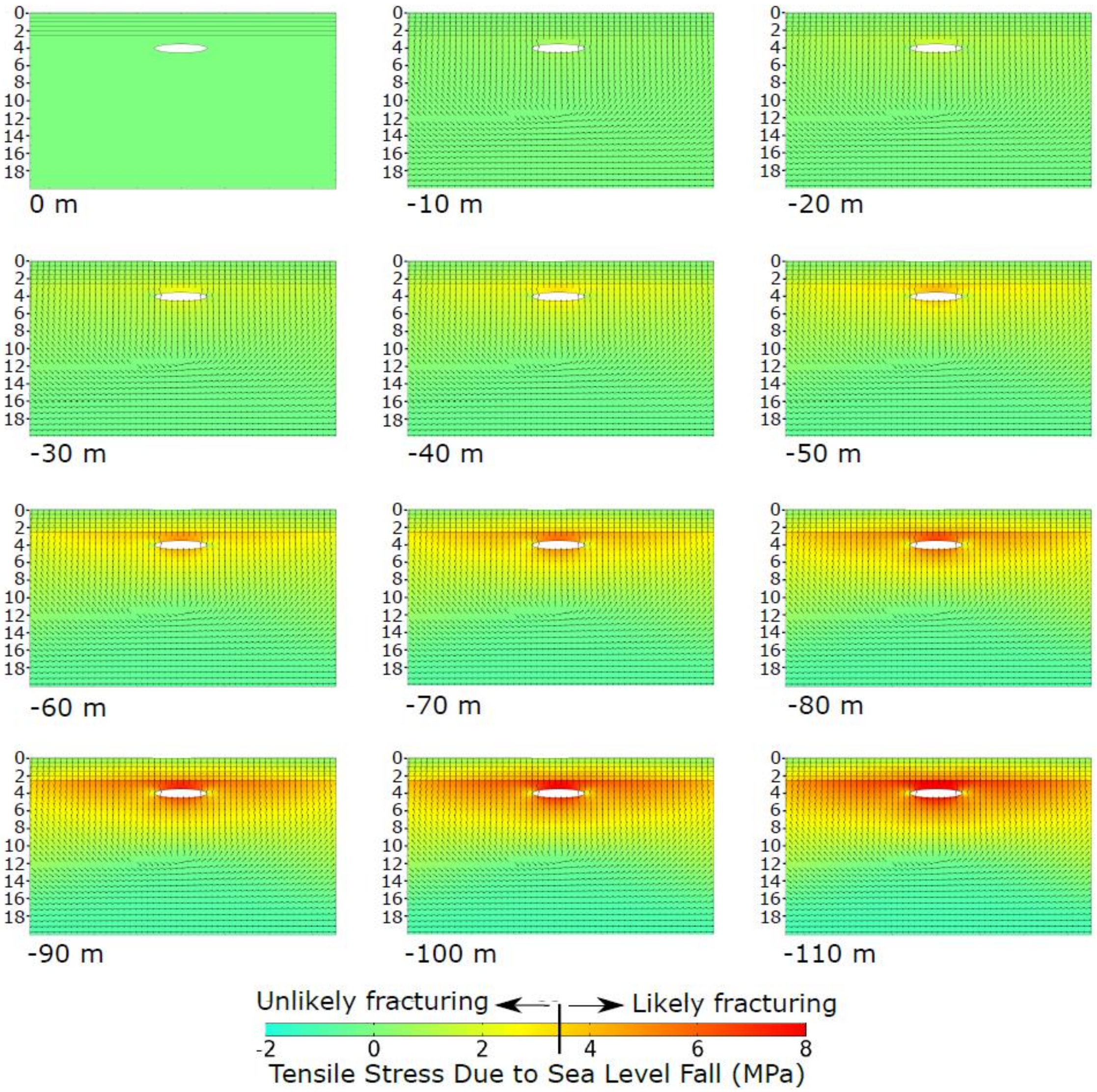

Figure 2. Numerical model of the increase in tensile stress around Santorini's shallow magma chamber (white elliptical hole) induced by sea-level fall in 10 m increments. Vertical scale indicates km below the surface. Red and yellow/orange areas indicate locations where tensile stress is likely to encourage dyke injection. Models with sea-level at -40 m (below the present level) or lower yield tensile stresses of > 3.5 MPa (the average crustal tensile strength), encouraging rupture of the magma-chamber roof and dyke injections. Initially (i.e. at -40 m), the induced tensile stress are limited to the margins of the chamber (host rock close to the chamber), so that the dykes would propagate only for a short distance and then become arrested. As the sea-level continues to fall the induced tensile stress spreads throughout the roof. When the sea-level has reached -70 m to -80 m, induced tensile stress occurs in much of the roof, whereby the first feeder-dykes in the sea-level cycle are generated (cf. Fig. 3). There are 5 layers above the magma chamber, each 500 m thick. The abrupt increase in Young's modulus between the fifth layer and the layer hosting the chamber is the reason for the notable tensile-stress concentration under the contact between these layers (the stress concentrates in the stiff layer/unit hosting the chamber). Full model parameters are disclosed in the Methods section.

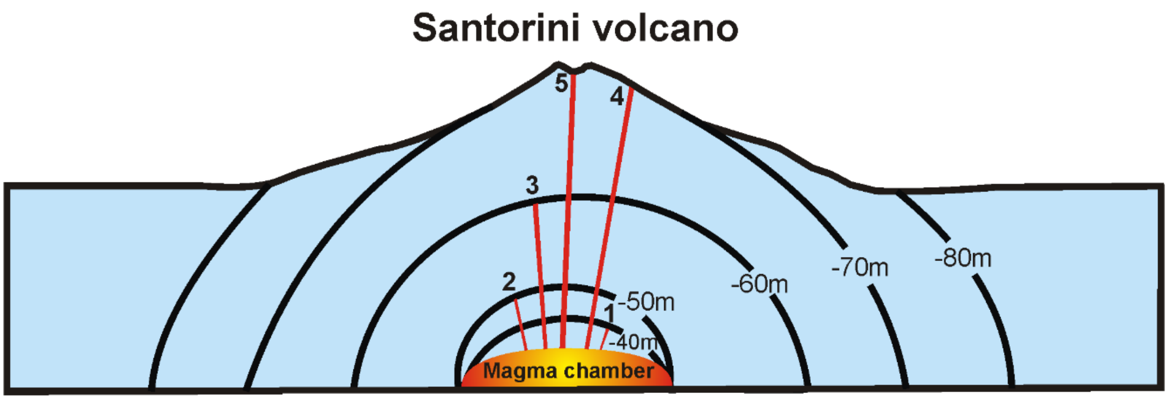

Figure 3. Schematic illustration of the spreading of the sea-level induced tensile stress in the roof of the magma chamber of the Santorini volcano and its effect on the propagation of injected dykes. The limits of the zones (marked by thick black semi-circular/semi-elliptical curves) within which induced tensile stresses favour dyke propagation for a given sea-level are indicated. The indicated sea-levels below the present one are -40 m, -50 m, -60 m, -70 m, and -80 m. Schematic propagation paths of five dykes (red straight lines), numbered 1 to 5, are shown. When the sea-level has fallen to -40 m, induced tensile stress is limited to a semi-elliptical zone close to the chamber (the outer boundary of the zone is the -40 m curve) and all injected dykes (represented by dyke 1) become arrested. When the sea-level falls further, tensile stress spreads through the roof of the chamber, but at levels -50 m and -60 m the outer boundaries of the high-tensile stress zones are still well below the surface, so that injected dykes (represented by dykes 2 and 3) become arrested. However, when the sea-level falls to -70 m and, particularly, -80 m, induced tensile stresses reach to the surface of the volcano, and dyke-fed eruptions (represented by dykes 4 and 5) begin.

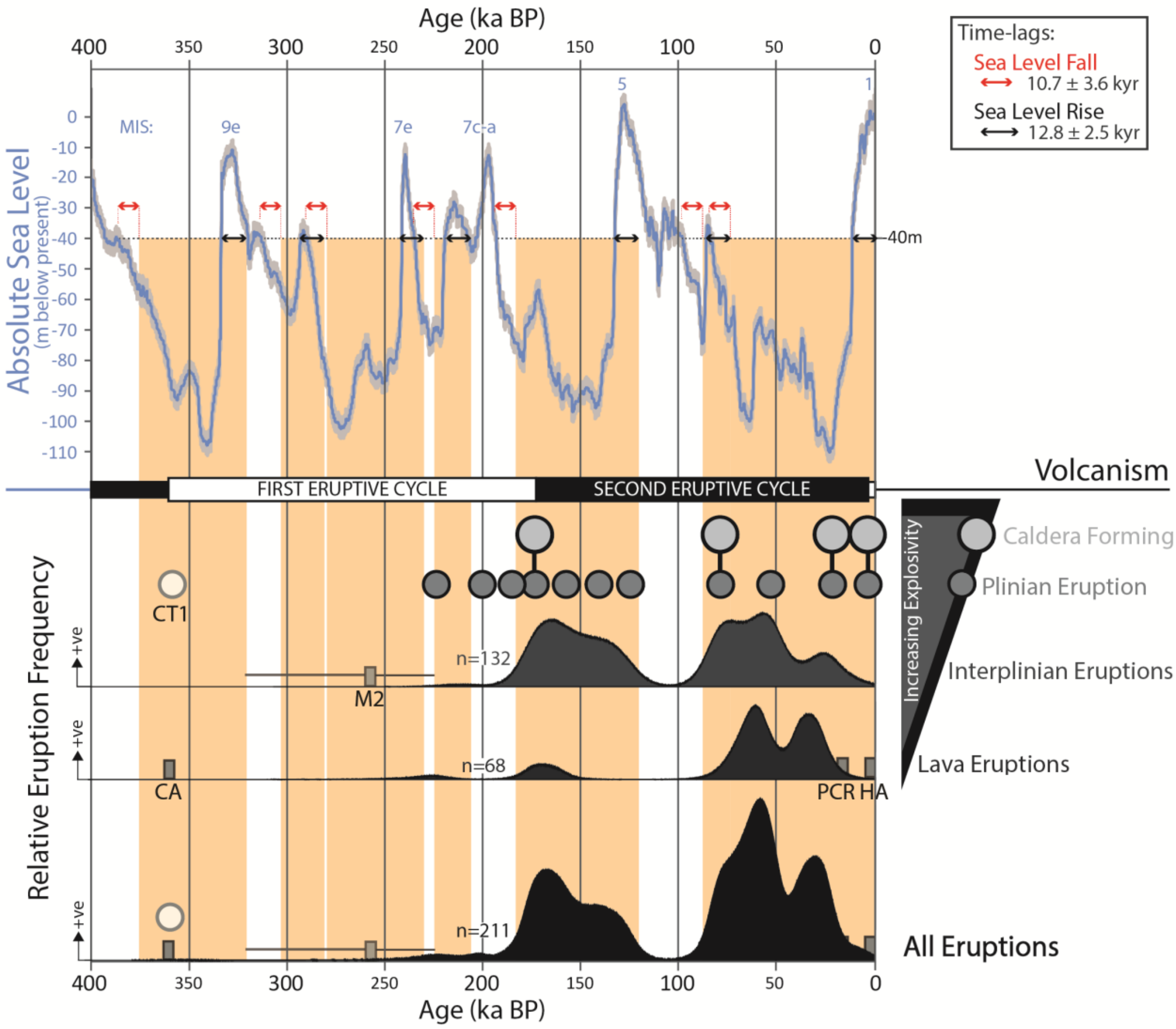

Figure 4. Santorini's eruptive stratigraphy (lower panels) aligned to the P_{max} absolute sea-level (blue curve with grey 95% confidence interval)[23,24]. Where both the chronology and the number of eruptions are well constrained, the eruption time series (lower half of diagram) is represented by kernel density estimates (grey/back) with the number of events of each type shown (total n=211). Where the number of events is either difficult to determine or the dating is very imprecise, eruptive events have been represented in grey boxes or circles (most likely date) with whiskers for the error (if known). The height of the boxes does not imply the number of events. These events are labelled to allow simple reference to the existing literature; CT1= Cape Therma 1, CA=Cape Alai Lavas, M2= interplinian deposits[44,45]. PCR=Post Cape Riva lavas and HA= Historical Activity. Time-lags between the sea-level falling or rising through -40 m and the start or end of eruptive activity are denoted by red and black arrows respectively. See text for full explanation. Also shown are the time periods of the eruptive 'cycles' which are traditionally used to describe the cycles in composition and style of Santorini's eruptions.

Methods

The eruption stratigraphy

The volcanic stratigraphy of Santorini is unrivalled in its detail and exposure. Three forms of eruptive activity are examined from the exposed stratigraphy: 1) Plinian activity[1,2]; 2) interplinian activity[2-4], and 3) lavas[5,6]. The numbers of eruptions of each type used in this study (Supplementary table 1) have been compiled from the evidence set out in these previous stratigraphic studies. The tephrochronology of the island[7] forms the main framework of the chronology but is here supplemented by other forms of geochronology[2,8-11].

Note on the preservation of interplinian explosive eruptions

Deposits from smaller interplinian events can be locally absent, depending on the wind direction and topography at the time of eruption. This could result in the preserved stratigraphy under-representing the number of eruptions. Furthermore, one eruption could produce two or more superimposed but distinct deposits, in which case simply counting the deposits within a stratigraphy would over-estimate the number of eruptions. To accommodate these uncertainties as far as possible we have estimated the number of interplinian eruption events in each interval in three ways, using three different assumptions.

The first estimate assumes that each pyroclastic deposit in the most complete exposure available for a particular time interval represents a separate eruption event, giving a maximum estimate for the number of events. However, a single eruption may produce several superimposed deposits and these counts would therefore overestimate of the number of eruptions. The second estimate is the already published interpretation of the number of discernible individual eruptive events[3,4,6]. However, this method relies on the qualitative judgement of several different authors, as different parts of the stratigraphy have been reported in different papers. The third method defines a minimum estimate by using only palaeosols and weathering horizons to define a minimum number of events and disregards the number of discrete volcanic deposits altogether. For example, if a stratigraphic section has two palaeosols evident in it, the number of eruptive events would be estimated as three.

Importantly, regardless of the method used, time intervals where there are no deposits evident in the stratigraphy will always yield 0 as an estimate for the number of events. As this paper explains the mechanisms controlling the start and end of periods of volcanic activity (some eruptions) and periods of quiescence (no eruptions), our conclusions are not affected by using a different estimate of the number of interplinian eruptions. We use the first method (maximum estimate) in our comparison to the sea-level record (main text Fig. 4) as it is the only method which can be applied across the entire time sequence (Supplementary tables 1 and 2) and also provides the best contrast between periods of activity and periods of quiescence.

Note on preservation of lava eruptions

The eruption history as represented in the caldera walls, while highly detailed, is inevitably incomplete[2]. Material from explosive tephra (ash or pumice) producing eruptions can be carried to and preserved within the caldera wall stratigraphy, but lavas will only become preserved within the peripheral stratigraphy when the intra-caldera island is large enough allow the lavas to on-lap the caldera walls. The peripheral stratigraphy therefore omits some periods of intra-caldera lava shield eruptions. Where smaller intra-caldera islands are known from other evidence such as lithics in the deposits of subsequent eruptions[9] this information has been added qualitatively to figure 4, but clearly the number of these events cannot be quantified. It could be argued that small intra caldera islands existed during the periods where we have no eruptions recorded in our dataset. However, for the two major hiatuses identified in the eruptive record (main text Fig. 4), the field evidence summarised below implies that this is not the case.

Firstly, for the period between the Cape Therma 2 and 3 eruptions (main text figure 2 and 4), rhyodacite lava flows at Cape Alonaki and NE Thera are preserved immediately following the Cape Therma 2 eruption. However, there are no such lavas following the Cape Therma 3 eruption. As there is no evidence of a caldera forming event during this period, there is no reason to believe that any lavas would be prevented from being preserved within the caldera walls by the formation of a caldera following the Cape Therma 3 eruption. We therefore infer that the absence of lavas following the Cape Therma 3 eruption reflects a period without major effusive volcanic activity, rather than just an absence of evidence.

Secondly, immediately following the Vourvoulos eruption, which was not associated with caldera collapse (main text Figs 1+4), there is also no evidence of lava deposition. Again, this is unlikely to be due to a lack of preservation. Lavas of the Simandiri shield are evident in the caldera wall stratigraphy after the Lower Pumice 2 eruption (Main Text Fig. 1) and there is no evidence for a significant caldera forming event between these and the Vourvoulos eruption showing that the intra caldera island was large enough for any post-Vourvoulos lavas to have surmounted the peripheral topography and be preserved.

The eruption chronology

The chronology of Santorini's eruptions has been recently been reviewed and updated[7] and this forms the basis of the dataset used here. Chronological constraints on the eruptive history of Santorini used here are a compilation of $^{40}K/^{40}Ar$ and $^{40}Ar/^{39}Ar$[2,6] as well as radiocarbon dates[6,8], and tephrochronological dates for geochemically matched ash layers found in marine sediment cores which are based on interpolation of sapropel core chronologies[7]. These are defined in Supplementary table 1.

A major strength of our methodology is that all but one (the Cape Therma 2 eruption) of the tephrochronological dates[7] are derived from the same age model which defines the chronology of the sea-level curve[12] and do not therefore carry the uncertainty which would otherwise be inherent in the fusion of two or more types of chronologies. They are derived from three marine sediment cores (KL49, KL51 and LC21), located South East of Santorini ([7]Supplementary Information Figure 1).

This high precision and detailed chronological framework is supplemented by additional events known from the Santorini proximal stratigraphy. These have less precise ages and/or it is not possible to estimate the numbers of eruptive events as some of the deposits relating to these events are exposed in inaccessible areas of the caldera, or have been removed by caldera formation (such as the proposed intra-caldera island that existed after the Cape Riva eruption and before the Minoan/Late Bronze Age eruption[9]. These data are shown in table 2.

Kernel Density Estimates of the eruptive record between 0 and 224 ka.

The eruption chronology between 0 and 224 ka is well constrained by dates from marine tephrochronology, K-Ar, Ar:Ar and radiocarbon methods. These provide a precise framework for the eruptive record but most of the individual lavas and interplinian deposits within the record are not directly dated. In order to deal with this we have set up a Bayesian chronological model constrained by the major dated events. The major dated events are treated as boundaries for phases of volcanic activity or in some instances phases of repose for the volcanic system. The approach taken is now standard practice within radiocarbon chronological research[13]. The major dated events (closed circles) used to constrain the chronology and the phases or periods which follow (open circles) are from oldest to youngest:

- Start M2 (rhyodacite lava)
    - M2
- Cape Therma 2 and Alonaki Lavas Base
    - M3
- Cape Therma 3
    - M4
- Lower Pumice 1
    - M5
- Lower Pumice 2
    - M6 (including Simandiri Lavas at 172+-4ka)
- Cape Thera Ignimbrite
    - M7
- Middle Pumice
    - M8 (including Megalo Vouno)
- Vourvoulos
    - M9
- M9-2
    - Repose Period (with Palaeosol)
- Upper Scoria 1
    - M10a
- Skaros Lavas base
    - Skaros Lavas
    - M10b
- Upper Scoria 2
    - M11a
- Lower Therasia Andesite
    - Repose Period
- Theresia Lavas base
    - Therasia Lavas
- Theresia Lavas top
    - M11b
- Cape Riva
    - M12

- Minoan/Late Bronze Age Eruption

The periods M2 to M12 refer to the interplinian periods[4]. Within the periods or phases we assume that the identified lavas and interplinian events can take any date between the bracketing dated events. We also assume where relevant, within the age uncertainties, that the dated events are constrained to be in the order listed above.

We use a Markov Chain Monte Carlo (MCMC) approach to generate multiple (480000) scenarios consistent with this model and use simple Kernel Density Estimate (KDE) plots (as defined by KDE_Plot[13]) to summarise the distribution of different types of volcanic activity over time from the MCMC scenarios. We generate KDEs for lavas (n=68), interplinian events (n=132), and all volcanic activity (lavas, Interplinian and Plinian events = 211) and these are shown with the sea-level record in figure 4. The number of Plinian eruptions by themselves (n=11) is too low to be useful for a KDE plot so we show these on figure 4 in the main text as individual events.

The advantage of using a Kernel Density Estimate is that it does not require arbitrary binning and so should provide the most realistic estimate of the temporal distribution of identified events. It also accommodates quantified age uncertainties which may overlap the boundaries of arbitrarily defined time bins. It should be noted that we are not able to overcome any biases that might come from the differential survival of the remnants of events from different periods which would affect our identification tallies. For example, minor events are more likely to be detectable for recent periods than for the older end of the time range. This should not affect our overall thesis which concerns the mechanisms controlling the start and the end of periods of eruptions or quiescence, but it does preclude undertaking a correlation analysis between absolute sea level and the number of eruptions in the manner of other studies[14,15].

The analysis was carried out using the OxCal software package v4.3.2[13,16]. Model code is given in the supplementary file which can be used to rerun and check the results of this paper.

Modelling the effect of Quaternary sea-level changes on Santorini volcano

Here we model (Supplementary Information Figure 2 and main text Figure. 2) the effects on tensile stress induced around the shallow magma chamber of Santorini volcano by crustal unloading due to removal of 110 m depth of sea water, simulating the change from Quaternary sea level maxima to minima. Our model assumes elastic behaviour of the host rock under stationary (non-dynamic) conditions, in order to effectively isolate the elastic component of the tensile-stress imposed by sea-level change. As the sea-level falls the load on the crustal decreases, inducing tensile stress around the chamber; as sea-level rises again the load on the crust increases, resulting in suppression of the induced tensile stress. The load is here the vertical stress due to the hydrostatic pressure of the sea water. Hydrostatic pressure p is given by $p = \rho g z$ where ρ is the sea-water density, g is the acceleration due to gravity, and z is the depth below the sea-level. Because the average density of sea water is about 1025 kg m^{-3} and the acceleration due to gravity about 9.8 m^{-2} it follows that for every 10 m of sea level rises/falls, the hydrostatic pressure or vertical stress changes by about 0.1 MPa. These pressure changes are applied in 10 m intervals to a COMSOL crustal flexure model (Supplementary Information Figure 1 and main text Fig. 2) comprising an anisotropic medium with layers above the shallow magma chamber. The edge of the models are fixed (fastened) while the surface of the model is free to accommodate surface deformation. The modelled crustal segment is 20 km thick and 100 km wide, so that the lateral edges are far from the shallow magma chamber (avoiding any edge effects on the calculated local stress field around the chamber) which is located at 4 km depth, reflecting known geophysical observations[17,18]. Six 500 m thick layers are included above the magma reservoir to accommodate surface layering or stratigraphy. Material properties of these layers are: Poisson's ratio = 0.25 and density = 2700 kg/m^3. Young's modulus increases from surface layer to the rock layer hosting the shallow chamber as follow: surface layer (5 GPa), second layer (10 GPa), third layer (15 GPa), fourth layer (20 GPa), fifth layer (30 GPa) and the rock layer/unit hosting the magma chamber (40GPa).

Methods References

1. Druitt.T.H et al. Explosive volcanism on Santorini, Greece. *Geol. Mag.* **126,** 95-126 (1989).

2. Druitt, T.H., et al. Santorini volcano. Geol. Soc. Lond. Mem. 19, 1-165 (1999).

3. Edwards, L., Magma cyclicity and isotopic variation on Santorini volcano, Aegean Sea, Greece. Ph.D. Thesis University of Bristol, UK (1994).

4. Vespa.M et al. Interplinian explosive activity of Santorini volcano (Greece) during the past 150,000 years. *J. Volcanol. Geoth. Res.* **153,** 262-286 (2006).

5. Huijsmans, J.P.P. and Barton, M. Volcanoes from Santorini, Aegean Sea, Greece: Evidence for Zoned Magma Chambers from Cyclic Compositional Variations. *Journal of Petrology* **30** pp. 583-625 (1989)

6. Fabbro, G., Druitt, T.H., Scaillet, S. Evolution of the crustal magma plumbing system during the build-up to the 22-ka caldera forming eruption of Santorini (Greece), *Bull Volcanol*. 75:767 DOI 10.1007/s00445-013-0767-5 (2013).

7. Wulf, S., et al. Advancing Santorini's tephrostratigraphy: new glass geochemical data and improved marine-terrestrial tephra correlations for the past ~360 kyrs. *Earth Sci. Rev.*, https://doi.org/10.1016/j.earscirev.2019.102964 (2020).

8. Manning, S.W., et al. Chronology for the Aegean Late Bronze Age 1700-1400 B.C. *Science* **312** pp 565-569 (2006)

9. Karátson, D. et al. Towards reconstruction of the lost Late Bronze Age intra-caldera island of Santorini, Greece. *Nature Sci. Rep* **8**. (2018) https://doi/10.1038/s41598-018-25301-2.

10. Vakhrameeva, P. et al. The cryptotephra record of the Marine Isotope Stage 12 to 10 interval (460-335 ka) at Tenaghi Philippon, Greece: Exploring chronological markers for the Middle Pleistocene of the Mediterranean region. *Quat. Sci. Rev*. **200**, 313–333 (2018).

11. Vakhrameeva, P., et al. Eastern Mediterranean volcanism during Marine Isotope Stages 9 to 7e (335–235 ka): Insights based on cryptotephra layers at Tenaghi Philippon, Greece. *J. Volcanol. Geoth. Res*. **380**, 31–47 (2019).

12. Grant et al. Sea-Level variability over 5 glacial cycles. *Nature Commun.* **5**.5076 DOI: 10.1038/ncomms6076 (2014).

13. Bronk Ramsey, C. Bayesian analysis of radiocarbon dates. *Radiocarbon*, **51**(1), 337-360. doi:10.1017/s0033822200033865 (2009).

14. Kutterolf, S. et al. Milankovitch frequencies in tephra records at volcanic arcs: The relation of kyr-scale cyclic variations in volcanism to global climate changes. *Quart. Sci. Rev.* **204**, 1-16 (2019).

15. Sternai, P., et al. Magmatic pulse driven by sea-level changes associated with the Messinian salinity crisis. *Nat. Geo.* DOI: 10.1038/NGEO3032 (2017).

16. Bronk Ramsey, C. Methods for Summarizing Radiocarbon Datasets. *Radiocarbon*, **59**(2), 1809-1833. doi:10.1017/rdc.2017.108 (2017).

17. Parks, M.M. et al. Evolution of Santorini volcano dominated by episodic and rapid fluxes of melt from depth. *Nature Geosci.* **5**, 749-754 (2012).

18. Parks, M.M., et al. From quiescence to unrest - 20 years of satellite geodetic measurements at Santorini volcano, Greece. *J. Geophys. Res.* (Solid Earth), **120**, 1309-1328, doi:10.1002/2014JB011540 (2015).

19. Simmons et al. The initiation and development of a caldera-forming Plinian eruption (172 ka Lower Pumice 2 eruption, Santorini, (Greece). *J. Volcanol. Geoth. Res.* 10.1016/j.jvolgeores.2017.05.034 (2017).

20. Gertisser. R. and Wiltshire, R. Explosive volcanic activity during the evolution of the Skaros lava shield, Santorini, Greece. Conference Abstract, Cities on Volcanoes Naples (2018).

21. Vaggelli et al., Highly Sr radiogenic tholeiitic magmas in the latest inter-Plinian activity of Santorini volcano, Greece. *Journal of Geophysical Research* **114** doi:10.1029/2008JB005936

22. Gudmundsson, A. Rock fractures in geological processes. Cambridge Univ. Press, Cambridge, 2011.

23. Browning**.** et al. Forecasting magma chamber rupture at the Santorini Volcano, Greece *Nature Sci. Rep.* **5**, 15785 DOI: 10.1038/srep15785 (2015).

24. Grant et al. Rapid coupling between ice volume and polar temperature over the past 150,000 years. *Nature* **491**, 744-747 (2012).

25. McGuire et al. Correlation between rate of sea-level change and frequency of explosive volcanism in the Mediterranean. *Nature* **389** pp473-476 (1997).

26. Quidelleur et al. Causal link between Quaternary paleoclimatic changes and volcanic islands evolution *Geophys. Res. Lett.* **35**, L02303 doi:10.1029/2007GL031849 (2008)

Supplementary Information.

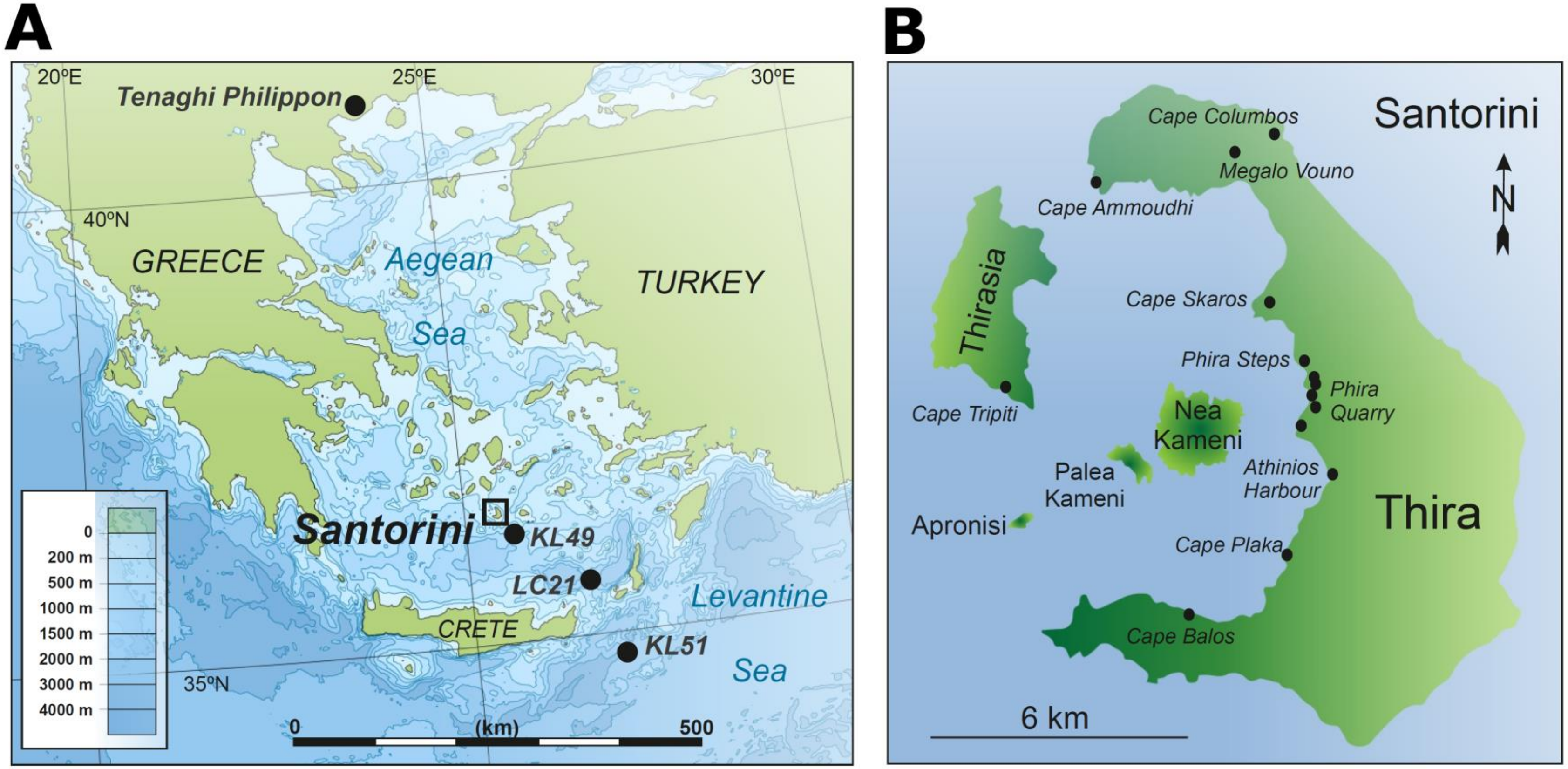

Supplementary Figure 1. (after Wulf et al., 2019) A) Map showing the location of Santorini (black box) and of the marine cores (black dots) which contribute both the sea-level record (core LC21) and the tephrochronology dates for the Plinian eruptions which constrain Santorini's eruption history (KL49, KL51, LC21- from 20). B) The islands of Santorini and the locations of stratigraphic sections contributing to Santorini's chronology and eruption count estimates 43, 44, this study. While the palaeostratigraphy is derived from locations in the caldera wall (Thera and Therasia islands), the central island of Nea Kameni is the location of historical eruptive activity (after the Late Bronze Age Eruption at 3.6 ka),

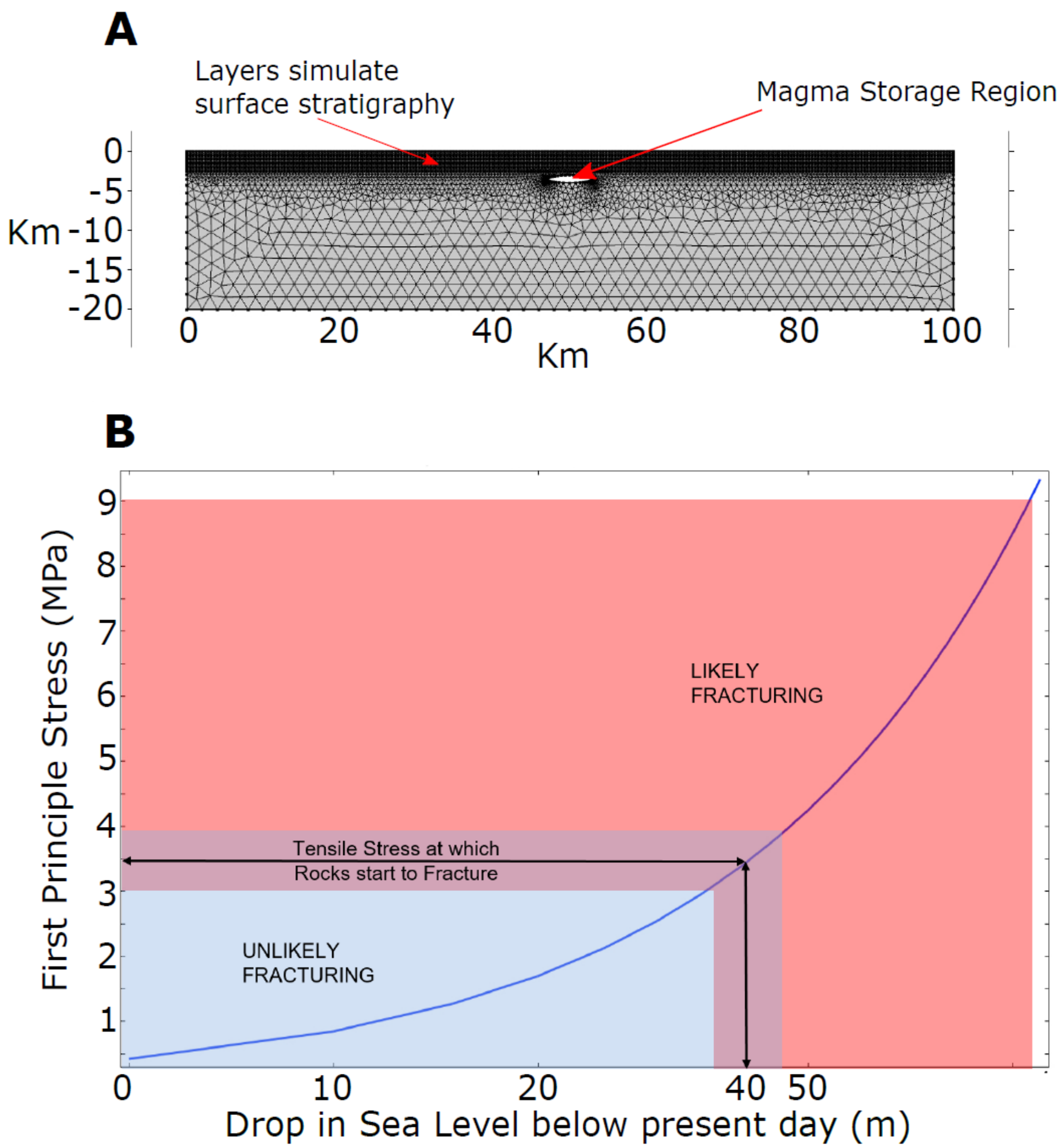

Supplementary Figure 2: A) shows the COMSOL model geometry B) Graph shows the relationship (blue line) between the first principle (tensile) stress at the top of the magma storage region and the fall in sea level below the present day. Note the x-axis is exponential, creating a curved line. The relationship between the first principle stress and the drop in sea level is actually linear in an elastic model. The likely range of tensile strengths (tensile stress at which rocks start to fracture) is between 3 and 4 MPa[22,23] with an average of 3.5 MPa, this defines our modelled prediction that a 40 m drop in sea level being large enough to allow magmatic excess pressure p_e (see equation in the main text) to fracture the roof of the magma reservoir and for dykes to begin to propagate.

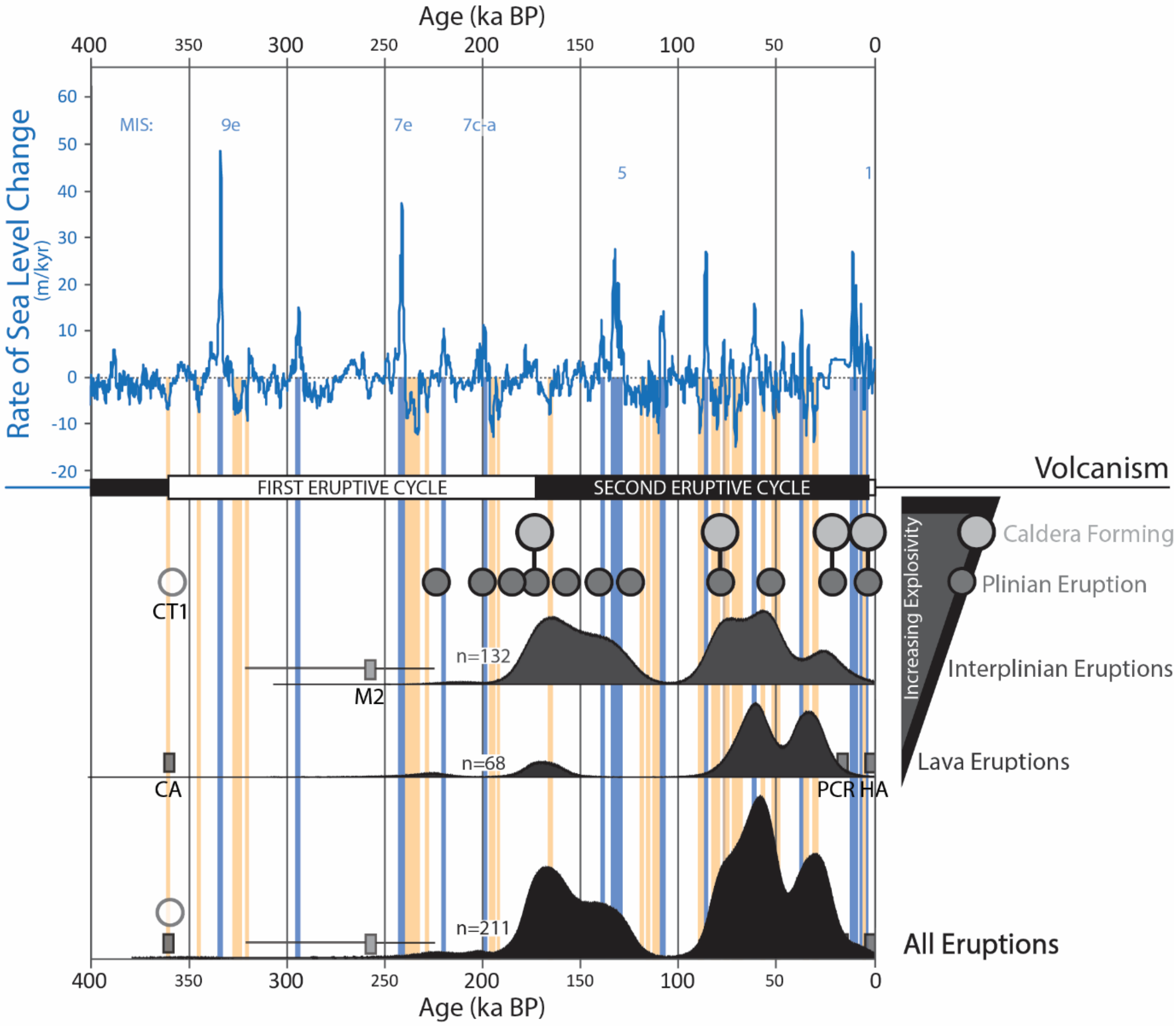

Supplementary Figure 3. Santorini's eruptive stratigraphy (lower panels) aligned to the P_{max} rate of sea-level change (blue curve)[12,24]. Where both the chronology and the number of eruptions are well constrained, the eruption time series (lower half of diagram) is represented by kernel density estimates (grey/back) with the number of events of each type shown (total n=211). Where the number of events is either difficult to determine or the dating is very imprecise, eruptive events have been represented in grey boxes or circles (most likely date) with whiskers for the error (if known). The height of the boxes does not imply the number of events. These events are labelled to allow simple reference to the existing literature; CT1= Cape Therma 1, CA=Cape Alai Lavas, M2= interplinian deposits[3]. PCR=Post Cape Riva lavas and HA= Historical Activity. Vertical beige bars denote time periods of rapid sea level fall (>8m/kyr), whereas vertical blue bars indicate times of rapid sea-level rise, phenomena previously proposed as a potential influence on volcanic activity[25,26]. At Santorini, there does not appear to be any relationship between the timing or type of volcanic activity and the rate of sea-level change.

Date/deposit type Plinian = major explosive eruption Interplinian = minor explosive eruption Lavas= individual lava flows	Dated horizon or interval name (nomenclature follows previous studies[2,4])	Date (ka)	Date 2SD	Number of lavas	Maximum estimate of number of interplinian units in most detailed stratigraphic section available (used as estimate for number of events- Main Text Fig.4)	Estimate of number of interplinian events from the number of correlated interplinian deposits	Minimum estimate of number of interplinian events (from palaeosol/weathering horizon evidence)	Comments/dating method	Reference
Plinian + 2 Lavas	Cape Therma 2 and lowest Alonaki lava	224	10	2	0	0	0	K/Ar Also a date of 257+62 ka from related lava in Rhyodacites of NE Thera 2 is a minimum number of lavas[2]	2
Interval	M3	-	-	0	1	1	1	This single interplinan deposit is separated from the Cape Therma 2 by weathering horizon and is so thought to occur after the Alonaki lavas, as these are contemporary with the Cape Therma 2 Plinian eruption.	Observation- this study.
Plinian	Cape Therma 3	200.2	0.9	0	0	0	0	Tephrochronology	7
Interval	M4	-	-	0	0	0	0	There are layers at the base of LP1, which are described as “precursors of LP1”[19]; we therefore count them as belonging to the same eruptive event as LP1 at 185.7 ka and not in this interval.	2
Plinian	Lower Pumice 1	185.7	0.7	0	0	0	0	Tephrochronology	7
Interval	M5	-	-	0	0	0	0	-	2
Plinian	Lower Pumice 2	176.7	0.6	0	0	0	0	Tephrochronology	7
Lava	Lowermost Simandiri Lava	172	8	1	0	0	0	Ar/Ar	2
Interval	M6 (including Simandiri Lavas at 172+-8ka)	-	-	6	29	10	16	-	3

Plinian	Cape Thera	156.9	2.3	0	0	0	0	Tephrochronology	7
Interval	M7	-	-	0	15	5	3	-	3
Plinian	Middle Pumice	141.0	2.6	0	0	0	0	Tephrochronology	7
Interval	M8	-	-	0	14	9	7	-	4
Plinian	Vourvolous	126.5	2.9	0	0	0	0	Tephrochronology	7
Interval	M9 (including Cape Columbos Tuff)	-	-	0	2	1	2	-	4,7
Interplinian eruption event	M9-2	121.8	2.9	0	1	0	0	Tephrochronology	7
Interval	Repose Period (with Palaeosol)	-	-	0	0	0	0		N/A
Plinian	Upper Scoria 1	80.8	2.9	0	0	0	0	Tephrochronology	7
Interval	M10a (including Megalo Vouno Cinder Cone- inferred to occur synchronously with, or just after, Upper Scoria 1)	-	-	0	25	25	4	-	4,5,6,7
Lava	Skaros Lavas base	67	18	1	0	0	0	Ar/Ar	2
Interval	Skaros Lavas	-	-	29	10	10	10	No detailed logs exist for the interplinian eruptions in this interval so only a minimum estimate of the number of events can be defined	5,6,20
Interval	M10b	-	-	0	5	5	1	-	4
Plinian	Upper Scoria 2	54	6	0	0	0	0	Ar/Ar	2
Interval	M11a	-	-	2	15	6	2	-	4,6
Lava	Lower Therasia Andesite	48.2	2.4	1	0	0	0	Ar/Ar	6
Interval	Repose Period	-	-	0	0	0	0	-	N/A
Lava	Theresia Lavas base	39.4	2.2	1	0	0	0	Ar/Ar	6
Interval	Therasia Lavas	-	-	25	5	5	5	includes the Cape Tripiti pumice which is dated by Wulf et al. (2020) at 27.5 +/- 1.4 ka (Wulf et al., 2020)	6
Lava	Theresia Lavas top	24.6	1.3	1	0	0	0	Ar/Ar	6
Interval	M11b	-	-	0	8	5	3	-	4

Plinian	Cape Riva	22.0	0.6	0	0	0	0	Tephrochronology	7
Interval	M12	-	-	0	3	2	1	-	4,21
Plinian	Late Bronze Age (Minoan) eruption	3.6	0.8	0	0	0	0	Radiocarbon	8

Supplementary Table 1. Chronological constraints and estimates of the number of eruptions of each type through time used to create the Kernel Density Estimates shown in figure 4.

Date/deposit type	Dated horizon or interval name	Date (ka)	Date 2SD	Number of lavas	Number of interplinian events	Comments/dating method	Reference
Lavas and minor interplinian deposits	M1 interval- Cape Alai Andesites+ minor pyroclastics	Not known although and average K/Ar dates of, 345+/- 88 is reported for the Cape Alai lavas n Druitt et al., this date has large amounts of excess argon and large uncertainties as a result.	-	Unquantified but 60 m thick in caldera wall	Minimum of (2)-3 interplinian (felsic) eruptions (Vakhrameeva et al., 2018) and own observation; age relationship with Cape Alai lavas not clear. Minimum of 2 interplinian (mafic) eruptions (own observation).Unquantified	Constrained by date of overlying Cape Therma 1 eruption	2,10, This study
Plinian	Cape Therma 1 eruption	359	Not known	-	-	Dated by tephra preserved in a pollen stratigraphy (Tenaghi Philippon) in northern Greece. The pollen sequence shows that the eruption occurred during a glacial period (MIS 10) which is consistent with its occurrence during the sea-level low at ~350 ka (Fig. 4)	7, 10
Minor interplinian deposits	M2 interval	257	62	-	Minimum 2 (Vakhrameeva et al., 2019) but possibly as many as 8 eruptions (Wulf et al., 2020) based on the Tenhagi Philippon core.	There is little evidence on Santorini for a lot of eruptions in this interval, so 2 is more realistic, although correlations from Tenhagi Philippon cores to deposits on Santorini are still preliminary.	7,11
Lavas	Post Cape Riva (M12 interval)	20.2	2	Unknown, but lava shield estimated at 2.2–2.5 km^3.	-	Known and dated from lithic clasts preserved within the Minoan deposits. Age thought to represent beginning of the effusive activity after the Cape Riva eruption. This lava shield was destroyed during the Minoan (LBA) eruption and caldera formation.	9
Lava and Interplinian eruptions	Historical Activity	Post Minoan eruption (3.62 ka to present)	N/A	Minimum of 12 evident on	Unquantified	N/A	2, 17

				Nea and Palaea Kameni			

Supplementary Table 2. Evidence of eruptive activity at Santorini with either low chronological precision or unquantified numbers of deposits/events. These events are represented in grey on figure 4.